JACS
JOURNAL OF THE AMERICAN CHEMICAL SOCIETY

Article

pubs.acs.org/JACS

Core/Shell Colloidal Quantum Dot Exciplex States for the Development of Highly Efficient Quantum-Dot-Sensitized Solar Cells

Jin Wang,[†] Iván Mora-Seró,[‡] Zhenxiao Pan,[†] Ke Zhao,[†] Hua Zhang,[†] Yaoyu Feng,[†] Guang Yang,[§] Xinhua Zhong,*[,†] and Juan Bisquert[‡]

[†]Key Laboratory for Advanced Materials, Institute of Applied Chemistry, East China University of Science and Technology, Shanghai 200237, China

[‡]Photovoltaic and Optoelectronic Devices Group, Departament de Física, Universitat Jaume I, 12071 Castelló, Spain

[§]Electronic Materials Research Laboratory, Key Laboratory of the Ministry of Education & International Center for Dielectric Research, Xi'an Jiaotong University, Xi'an 710049, China

Supporting Information

ABSTRACT: Searching suitable panchromatic QD sensitizers for expanding the light-harvesting range, accelerating charge separation, and retarding charge recombination is an effective way to improve power conversion efficiency (PCE) of quantum-dot-sensitized solar cells (QDSCs). One possible way to obtain a wide absorption range is to use the exciplex state of a type-II core/shell-structured QDs. In addition, this system could also provide a fast charge separation and low charge-recombination rate. Herein, we report on using a CdTe/CdSe type-II core/shell QD sensitizer with an absorption range extending into the infrared region because of its exciplex state, which is covalently linked to TiO_2 mesoporous electrodes by dropping a bifunctional linker molecule mercaptopropionic acid (MPA)-capped QD aqueous solution onto the film electrode. High loading and a uniform distribution of QD sensitizer throughout the film electrode thickness have been confirmed by energy dispersive X-ray (EDX) elemental mapping. The accelerated electron injection and retarded charge-recombination pathway in the built CdTe/CdSe QD cells in comparison with reference CdSe QD-based cells have been confirmed by impedance spectroscopy, fluorescence decay, and intensity-modulated photocurrent/photovoltage spectroscopy (IMPS/IMVS) analysis. With the combination of the high QD loading and intrinsically superior optoelectronic properties of type-II core/shell QD (wide absorption range, fast charge separation, and slow charge recombination), the resulting CdTe/CdSe QD-based regenerative sandwich solar cells exhibit a record PCE of 6.76% (J_{sc} = 19.59 mA cm^{-2}, V_{oc} = 0.606 V, and FF = 0.569) with a mask around the active film under a full 1 sun illumination (simulated AM 1.5), which is the highest reported to date for liquid-junction QDSCs.

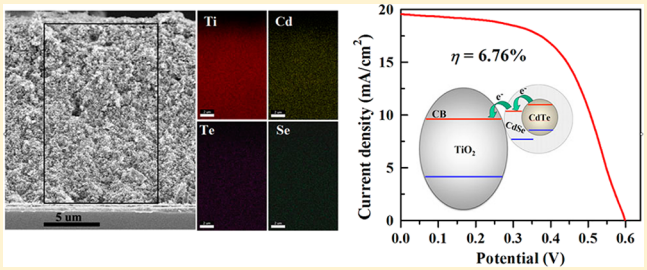

INTRODUCTION

The sustained increasing demand for energy and its effects on the environment greatly urges the efficient exploration of renewable clean energy, especially solar energy.[1] The quantum-dots-sensitized solar cell (QDSC) constitutes one of the most promising candidates for third-generation solar cells because of its various advantages, such as tunability of the band gap and high absorption coefficient as well as multiexciton generation (MEG)[2,3] and extraction of hot electrons,[4] which could boost the theoretical power conversion efficiency (PCE) beyond the Shockley–Queisser limit of 32%.[5−11] However, the potential of QDSCs has not been fully demonstrated, and the reported best PCEs are only on the level of 5−6% for liquid-junction and 10% for solid-state quantum-dot solar cells, respectively.[12−21] At least part of the reason for the low PCE is associated with the nature of the QD sensitizers used and the deposition method for tethering QD sensitizers onto a mesoporous oxide substrate, which causes a narrow light-harvesting range, inefficient charge separation, unwanted recombination, and low coverage of QDs.[5−11,22,23]

Searching suitable panchromatic QD sensitizers for expanding the harvest of solar light, enhancing charge separation, and retarding charge recombination is an effective way to improve the PCE of a QDSC.[22,23] To be an efficient sensitizers used in QDSCs, two important features should be considered: (i) the band gap of QD, which determines the light-harvesting range, and (ii) the conduction band edge, which affects the electron-extraction efficiency and charge recombination at the QD/electrolyte interface. Although utilization of QDs with a narrow band gap and/or large size can broaden the light-harvesting range, the electron-extraction efficiency is reduced because of the lower conduction band edge.[24,25] One possible way to simultaneously possess a wide absorption range, a fast electron

Received: August 2, 2013
Published: September 26, 2013

   dx.doi.org/10.1021/ja4079804 | J. Am. Chem. Soc. 2013, 135, 15913−15922

injection, and a low charge-recombination rate is to adopt type-II core/shell-structured QD sensitizers,[26−28] which are composed of a core-localizing hole and a shell-localizing electron. This spatial separation of charge carriers enables fast electron transfer from the QD sensitizer to the oxide matrix because of the enhanced electron density around the surface of the QD composite, which simultaneously suppresses the charge-recombination process because the shell acts as a tunneling barrier for the hole localized inside the core.[28] Another advantage of type-II QDs is the remarkable red shift of absorption edge because of the nature of "spatially indirect" energy gap, or exciplex state, offering an additional route to improve the spectral response by reducing the effective band gap.[26,29] All of these properties render type-II QDs as a satisfactory light-harvesting material for photovoltaic devices.

Despite the enormous potential of exciplex states in type-II QDs for the development of efficient photovoltaic devices, there are very few examples of its utilization. Among the few attempts to use a type-II core/shell QD (including ZnSe/CdS and ZnTe/ZnSe) as the light harvester in the context of photovoltaic devices,[30−33] all of the obtained PCE values are low (<3%), partly because of the narrow light-harvesting range of the QD sensitizers used[32,33] and/or the low QD loading.[30] Here, we explore a CdTe/CdSe type-II core/shell QD as a sensitizer in a QDSC. The absorption edge of CdTe/CdSe is readily tuned to the infrared spectral window, and the synthetic method has been well developed since the first colloidal synthesis by Bawendi's group.[26] It should be highlighted that infrared absorption is a promising feature for sensitizers in photovoltaic applications because half of the integrated power of the sun's power is located in the infrared spectral window. The efficient match of the sensitizer-absorption spectrum to that of the sun's power is an indispensible requirement for highly efficient photovoltaic devices.[34] Our recently developed postsynthesis assembly approach by the self-assembly of mercaptopropionic acid (MPA)-capped water-soluble QDs onto an oxide film electrode has been demonstrated to be an facile deposition route for high QD loading.[12−14] Furthermore, in comparison with the direct growth of QD onto a TiO_2 mesoporous film by successive ionic-layer adsorption and reaction (SILAR) or chemical-bath deposition (CBD) techniques,[16−18,35−41] the postsynthesis assembly approach (including direct adsorption,[42] linker-assisted assembly,[12−14,19,24,32,42−47] electrophoretic deposition route, etc.[48−50]) has many advantages because the size, surface functionalization, and consequently the surface trap and optoelectronic properties of the preprepared QDs can be conveniently controlled and tailored through the mature organometallic high-temperature synthetic method; these features directly determine the electron quenching, trapping, and recombining with the electrolyte in QDSC.[22,23,51]

Herein, high-quality infrared-absorption CdTe/CdSe core/shell QDs were prepared in organic media at high temperature according to a literature procedure.[52] The postsynthesis assembly approach using bifunctional linker MPA-capped water-soluble QDs, which were obtained via ligand exchange from the initial oil-soluble QDs, was adopted for tethering QDs on a mesoporous TiO_2 film through the formation of a covalent bond between capping ligand MPA and TiO_2 by dropping QD dispersions onto the TiO_2 film. With the combination of the intrinsically superior optoelectronic properties (wide spectral absorption, fast charge separation, slow charge recombination, etc.) of the adopted CdTe/CdSe type-II core/shell QD sensitizer as well as the effective deposition method for high QD loading, the resulting QDSC exhibits a record PCE of 6.76% with a mask around the active film under a full 1 sun illumination. Impedance spectroscopy (IS), photoluminescence (PL) decay, and intensity-modulated photocurrent/photovoltage spectroscopy (IMPS/IMVS) analysis have revealed faster electron injection and lower charge recombination, resulting in the more efficient charge collection of the CdTe/CdSe-based solar cells in comparison with the reference CdSe QD-based solar cells.

EXPERIMENTAL SECTION

Chemicals. Selenium powder (200 mesh, 99.99%), cadmium oxide (CdO, 99.99%), tellurium powder (200 mesh, 99.99%), 1-octadecene (ODE, 90%), trioctylphosphine (TOP, 90%), and oleyl amine (OAm, 95%) were obtained from Aldrich. Tetradecylphosphonic acid (TDPA, 98%) and oleic acid (90%) were purchased from Alfa Aesar. All reagents were used as received without any further purification.

Synthesis and Water-Solubilization of CdTe/CdSe Core/Shell QDs. A literature method with a two-step procedure was used to synthesize CdTe/CdSe QDs.[52] First, the 2.7 nm CdTe core with a first absorption onset at a wavelength of λ = 540 nm was prepared via the reaction of the CdO-TDPA complex with TOP-Te in ODE media at high temperature.[53] The SILAR strategy was adopted for the overgrowth of the CdSe shell on the preformed CdTe QDs. In a typical process, a chloroform solution of the purified CdTe QDs containing 0.1 mmol of CdTe, 0.5 mL of TOP, 70 mg of TDPA, and 3.5 mL of ODE was loaded in a round-bottomed flask, and the flask was evacuated at room temperature for 10 min and at 100 °C for another 10 min. Then, the reaction system was heated at 170 °C in an argon atmosphere for the deposition of CdSe. An equimolar amount of Cd and Se precursor solutions (0.1 M), obtained by dissolving $Cd(OAc)_2$ or elemental selenium in TOP/ODE (4:6, v/v), respectively, was added into the reaction system alternately at 30 min intervals. When the absorption spectra showed no further variation, another cycle of Cd/Se precursor solution was added repeatedly. After three cycles of Cd/Se overgrowth, 4.9 nm sized CdTe/CdSe core/shell QDs were obtained. The reaction mixture was dispersed in toluene and then purified by centrifugation and decantation with the addition of acetone. The reference CdTe and CdSe QDs with an identical particle size of 4.9 nm were also synthesized according to literature methods.[53,54] The MPA-capped water-soluble QDs were obtained via a ligand-exchange procedure by replacing the initial hydrophobic capping ligands (OAm and/or oleic acid) around the corresponding oil-soluble QDs with MPA according to literature methods.[12,55]

Construction and Characterization of QDSCs. TiO_2 mesoporous film electrodes were prepared by successive screen printing of a transparent layer (9.5 ± 0.5 μm) with the use of homemade P25 paste and a light-scattering/opaque layer (6.5 ± 0.5 μm) using 30 wt % 200−400 nm TiO_2 mixed with 70 wt % P25 paste over F:SnO_2 glass (FTO, 8 Ω/square) substrates followed by sintered in a muffle-type furnace at 500 °C for 30 min. A modification of the TiO_2 film with an aqueous solution of $TiCl_4$ (0.04 M) was then performed according to a typical procedure for dye-sensitized solar cells. The obtained TiO_2 film electrodes were then sensitized with the corresponding QDs sensitizers.

For tethering QDs on TiO_2 film electrodes, a drop of the MAP-capped QDs aqueous solution (30 μL, with an absorbance of 2.0 at 600 nm) was pipetted onto the TiO_2 film surface and remained there for 2 h before being rinsed with water and ethanol sequentially. A circular tape with a central hollow diameter of 6.0 mm was used to keep the QD solution on the TiO_2 film electrode. After finishing the deposition, the QD-sensitized TiO_2 film was treated with four cycles of ZnS by immersing into $Zn(OAc)_2$ and Na_2S aqueous solutions (0.1 M for both) for 1 min/dip alternately.

The Cu_2S counter electrodes were obtained by immersing brass foil in a HCl solution (1.0 M) at 70 °C for 5 min, which were then

dx.doi.org/10.1021/ja4079804 | J. Am. Chem. Soc. 2013, 135, 15913−15922

vulcanized by insertion into a polysulfide electrolyte solution for 10 min. The composition of the polysulfide electrolyte solution was 2.0 M Na_2S and 2.0 M S in distilled water. The solar cells were constructed by assembling the Cu_2S counter electrode and QD-sensitized TiO_2 film electrode with a binder clip separated by a Scotch spacer (50 μm thickness). Then, polysulfide electrolyte was filled inside the cell. For each QDSC studied, at least three cells were constructed and evaluated in parallel.

The photovoltaic performance ($J-V$ curves) of the QDSCs were evaluated using a Keithley 2400 source meter with illumination by a 150 W AM 1.5 G solar simulator (Oriel, model no. 94022A). The power of the simulated solar light was calibrated to 100 mW cm^{-2} with the use of an NREL standard Si solar cell. The photoactive area was 0.237 cm^2. In the process of measurement, a circular black metallic tape with a 6.0 mm diameter aperture, which is slightly larger than the photoactive region of 5.5 mm in diameter, was used as a shading mask.[56] The incident photon-to-current conversion efficiency (IPCE) spectrum was measured using a Keithley 2000 multimeter with illumination by a 300 W tungsten lamp with a Spectral Product DK240 monochromator. Impedance spectroscopy (IS) measurements were carried out with use of an impedance analyzer (Zahner, Zennium) under dark conditions at a different forward bias that ranged from 0 V to higher than V_{oc}, applying a 20 mV ac sinusoidal signal over the constant applied bias with the frequency ranging from 1 MHz to 0.1 Hz. $J-V$ curves were recorded before and after IS measurement to verify the validity of the IS data obtained. Intensity-modulated photocurrent spectroscopy (IMPS) and photovoltage spectroscopy (IMVS) spectra were recorded on a Zahner electrochemical workstation with a frequency-response analyzer under an intensity-modulated blue-light-emitting diode (30–150 W m^{-2}, 457 nm) driven by a Zahner (PP211) source supply. The modulated light intensity was 10% or lower than the base light intensity. The frequency range was set between 100 kHz and 0.1 Hz.

Characterization of QDs and Electrodes. Transition electron microscopy (TEM) measurements were performed on a JEOL JEM-1400 microscope. Scanning electron microscopy (SEM) was performed using an FEI Quatan250FEG SEM system equipped with an energy-dispersive X-ray (EDX) spectrometer. The absorption spectra of the QD dispersions and sensitized TiO_2 films (with dimensions of 2.0 × 1.0 cm^2) were measured using a Shimadzu UV-3101 PC UV–vis spectrophotometer. The PL emission spectra were recorded on a fluorescence spectrophotometer (Cary Eclipse Varian). The fluorescence lifetime study was carried out by an Edinburgh FL 900 single-photon counting system equipped with a picosecond light pulser (Hamamatsu C8898). The excitation light source was 441 nm laser light. A nonlinear least-squares fitting program was used to analyze the data, with the deconvolution of the excitation pulse being ~200 ps.

RESULTS AND DISCUSSION

Synthesis and Characterization of CdTe/CdSe Type-II Core/Shell QDs. A two-step organometallic high-temperature synthetic procedure was adopted for the preparation of high-quality CdTe/CdSe core/shell QDs with nearly uniform particle size and superior optical properties.[52] In the first step, 2.7 nm CdTe core QDs with a first absorption onset at 540 nm and a band edge PL emission at 558 nm were prepared according to a literature method.[53] In the next step, CdSe shells were then overgrown around the CdTe core template by alternately adding Cd/Se precursor to a dispersion of the purified CdTe core QDs at an intermediate temperature. The detailed procedure for the preparation of the CdTe core and CdTe/CdSe core/shell QDs is described in the Experimental Section. Figure 1a,b shows the wide-field TEM image of the CdTe core QDs (2.7 ± 0.2 nm) and the derivative CdTe/CdSe core/shell QDs (4.9 ± 0.3 nm) with three monolayers (ML) of the CdSe shell. Both the core and core/shell-structured QDs

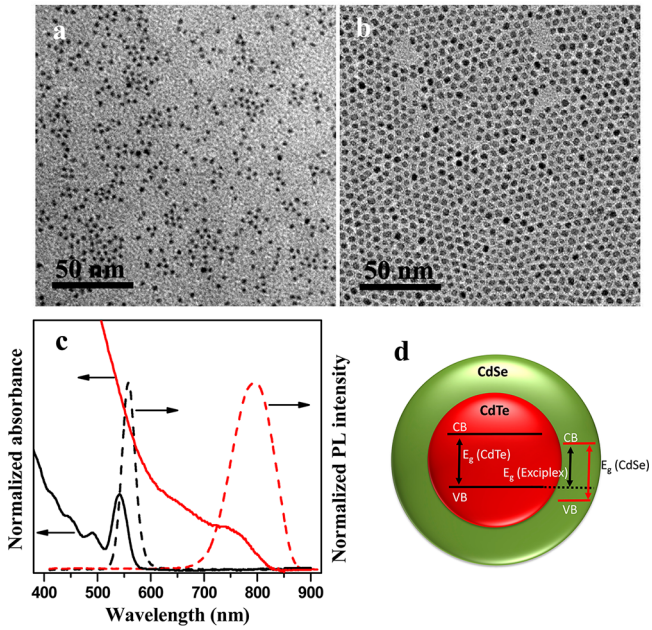

Figure 1. Structure and optical characterization of CdTe core QDs and derivate CdTe/CdSe core/shell QDs. (a, b) Wide-field TEM images of the initial 2.7 nm CdTe core QDs (a) and derivate 4.9 nm CdTe/CdSe core/shell QDs (b). (c) Corresponding normalized absorption (solid lines) and PL spectra (dashed lines, λ_{ex} = 360 nm) of CdTe (black lines) and CdTe/CdSe (red lines) QDs dispersions in toluene. (d) Cartoon of a core/shell CdTe/CdSe QD indicating the relative position of the bands. The conduction band (CB) and valence band (VB) are depicted with a solid black or red line for the CdTe and CdSe, respectively. The size of the band gap, E_g, for CdTe, CdSe, and the exciplex state (effective band gap) is indicated with arrows.

show a nearly dotted shape with a relative standard deviation σ = 4–6% without any size sorting. The photovoltaic performance of this size CdTe/CdSe core/shell QDs proved to be the best one in our experimental results. The optical spectra (absorption and PL emission) of the CdTe core and derivative CdTe/CdSe core/shell QDs are shown in Figure 1c. The CdTe core QD exhibits typical absorption and emission features, with a distinctive first excitonic absorption peak at ~540 nm and the band edge emission peak at ~558 nm. The distinctive peak in the spectra of CdTe cores is replaced by a featureless absorption tail into the red and infrared spectral window in the derivative CdTe/CdSe core/shell structures, and the corresponding PL emission peak red-shifted from 558 to 795 nm. It is noted that the observed huge spectral shift (237 nm) with the thin shell layer (3 ML) in the CdTe/CdSe system benefits from the use of a small-sized core. It has been demonstrated that large-sized cores cannot be effectively compressed through epitaxy, and as a result the PL emission spectra are much less tunable by lattice strain.[57] Such absorption and emission spectral features in the CdTe/CdSe core/shell QD suggest the existence of a type-II band arrangement. This is because type-II core/shell QDs effectively act as an indirect semiconductor near the band edges.[26,27] The band gap of a type-II core/shell structure thus depends on the band offsets of the two materials constituting the core and the shell, forming an effective band gap from the valence band of CdTe and the conduction band of CdSe (Figure 1d). This renders the band gap of type-II core/shell QDs smaller than that of either material. Correspondingly, the wavelengths of both the absorption onset and band edge PL emission of the

dx.doi.org/10.1021/ja4079804 | J. Am. Chem. Soc. 2013, 135, 15913–15922

type-II core/shell QDs are longer than those of either the core or shell QDs with identical sizes. For comparison, identically sized (4.9 nm) CdSe and CdTe QDs were also synthesized using literature methods, and their corresponding first excitonic absorption onsets were 610 and 670 nm, respectively (the corresponding spectra are shown in Figure S1 of the Supporting Information).[53,54] For simplification, the reference CdSe QDs specially refers to the 4.9 nm CdSe QDs with an excitonic onset at 610 nm hereafter. Therefore, the CdTe/CdSe type-II core/shell QDs enable us to extend the absorption onset to the infrared region, an unachievable target with either CdTe or CdSe QDs of an identical size. It should be highlighted that a small-sized QD with infrared absorption is a promising feature for sensitizers in photovoltaic devices because of the easy penetration into the mesoporous film and the high solar photon flux density in the infrared window.

Immobilization of QD Sensitizers onto TiO_2 Film Electrodes. The ex situ ligand-exchange postsynthesis assembly approach has been proven to be an effective route for tethering presynthesized QDs on a mesoporous TiO_2 film with high loading.[14] The initial hydrophobic ligands (mainly oleylamine/oleic acid) around the QD surface were replaced by a bifunctional hydrophilic ligand (MPA) in the ligand-exchange process; therefore, MPA-capped water-soluble QDs were obtained. The UV−vis absorption spectrum of MPA-capped CdTe/CdSe QDs aqueous solution is shown in Figure S2, which shows no significant change before and after phase transfer. The obtained MPA-capped water-soluble QDs were then tethered on TiO_2 electrodes according to a literature method by dropping a QD dispersion in water on the film and keeping it there for 2 h.[12−14] It is highlighted that the deposition of QDs onto mesoporous TiO_2 films is carried out at room temperature and under an ambient atmosphere. This renders the deposition procedure amenable to having a low-cost and high reproducibility.

Absorption spectra and corresponding photographs of the CdTe/CdSe and reference CdSe QD-sensitized TiO_2 films are shown in Figure 2. We can see that the spectral profiles of the QD aqueous dispersions were reserved after deposition on the TiO_2 films. This reflects the reservation of the particle size and freedom from particle aggregation. These features cannot be obtained by direct growth of QDs onto TiO_2 films in the reported literature.[16−18,35−41] The high absorbance of the sensitized film electrodes reflects the high loading amount of the QDs, which is also indicated by the deep color of the film electrodes, as shown in the inset of Figure 2. Because the excitonic absorption onset of the CdTe/CdSe QDs is featureless and there is no report for the corresponding extinction efficient, the exact value for the coverage of the CdTe/CdSe QDs around the TiO_2 film cannot be obtained on the basis of the absorption spectra of the sensitized film, but a loading amount as high as 34% coverage has been demonstrated in the case of CdSe-sensitized films based on this deposition method in our previous report.[14] The black color of the CdTe/CdSe-sensitized film indicates a nearly complete absorption of visible light. Furthermore, the light-harvesting range is expanded to a wavelength near 900 nm, as shown in the absorption spectra (Figure 2). The efficient harvesting of incident solar light paves the way for achieving a high photocurrent in the resulting cell devices, as described below.

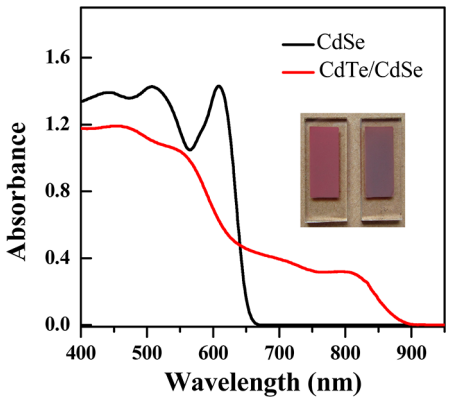

Figure 2. Diffuse reflectance absorption spectra of identically sized CdTe/CdSe and CdSe QD-sensitized TiO_2 film electrodes. Insets: photographs of CdTe/CdSe (right) and CdSe (left) QD-sensitized TiO_2 film electrodes.

Uniform Distribution of CdTe/CdSe throughout the Film. The cross-sectional SEM image for the CdTe/CdSe QD-sensitized TiO_2 mesoporous film electrode is shown in Figure 3a. It was found that the thickness of the transparent active TiO_2 layer is 9.5 ± 0.5 μm, and the thickness of the following scattering layer is 6.5 ± 0.5 μm. The uniform coverage of QDs around the mesoporous TiO_2 throughout the film thickness is verified by performing cross-sectional SEM with elemental mapping via EDX analysis. The elemental mapping on the rectangular area shown in Figure 3c−e demonstrates an excellently uniform distribution of Cd, Te, and Se atoms throughout the 16 μm thick mesoporous TiO_2 film. Atomic percentages from EDX elemental analysis on a cross section of the film were found to be 14.53 ± 0.25, 1.56 ± 0.06, 0.58 ± 0.04, and 1.12 ± 0.19% for Ti, Cd, Te, and Se, respectively. The Cd/Ti ratio from our postsynthesis assembly approach with use of MPA-capped water-soluble QDs is 0.11, which is in the same level as those (0.05−0.15) produced by the electrophoretic deposition method[48,49] but is pronouncedly higher than the value of 0.05 obtained by the linker-assisted assembly with the use of hydrophobic QDs.[58] The uniform distribution of the QDs as well as the high Cd/Ti ratio in our case gives solid support to the viewpoint that a nanometer-sized QD sensitizer can penetrate throughout the mesoporous film electrode depth with the use of MPA-capped QD aqueous dispersions.

Photovoltaic Performance. After the deposition of QD sensitizers, a thin ZnS passivation layer was then deposited onto the sensitized TiO_2 films by dipping them into the Zn^{2+} and S^{2-} aqueous solutions according to the normal literature procedure. The role of the deposition of a wide band gap ZnS layer is to reduce the internal recombination at QDs before charge injection as well as the charge recombination at the TiO_2/electrolyte and QD/electrolyte interfaces before charge injection and thus to improve the PCE.[23,59,60] Sandwich-type cells were constructed by assembling a QD-sensitized TiO_2 film electrode and Cu_2S counter electrode using binder clips, which was then filled with polysulfide electrolyte. Even though the use of methanol in electrolyte solutions can provide higher photocurrent, methanol is a nonregenerative hole scavenger, which is fatal for the long-term run of cell devices.[42] Therefore, no methanol polysulfide electrolyte was used in all of the tested cell devices. The $J-V$ curves of the CdTe/CdSe and reference CdSe cells under the illumination of an AM 1.5 G solar simulator with an intensity of 100 mW cm^{-2} (1 full sun) in the presence of masks are shown in Figure 4a, and the extracted

dx.doi.org/10.1021/ja4079804 | J. Am. Chem. Soc. 2013, 135, 15913−15922

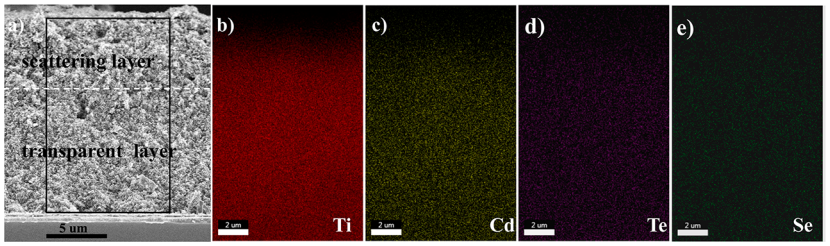

Figure 3. (a) Cross-sectional SEM image of a ~16.0 μm thick CdTe/CdSe-sensitized TiO_2 mesoporous film electrode consisting of a 6.5 μm scattering layer and a 9.5 μm transparent layer indicated by a dashed line. (b–e) Elemental mapping of titanium (b), cadmium (c), tellurium (d), and selenium (e) by EDX spectroscopy for the rectangular area indicated by the black box in panel a showing the uniform distribution of the CdTe/CdSe sensitizer throughout the film thickness.

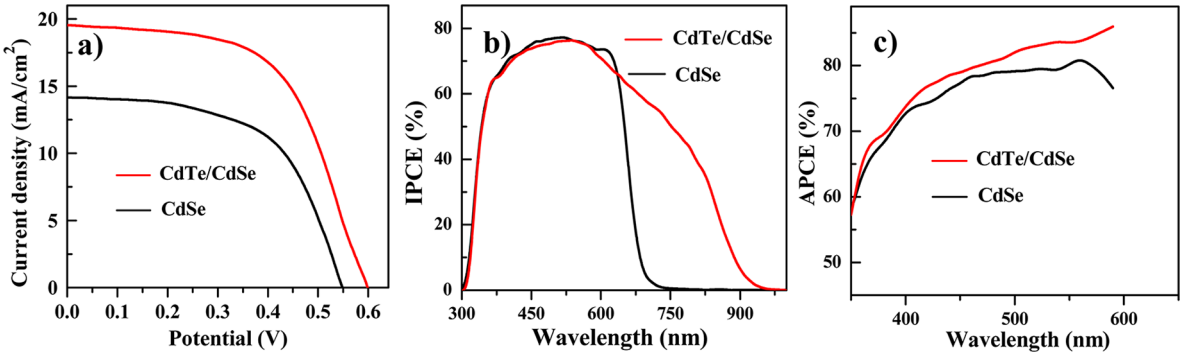

Figure 4. Photovoltaic performance of CdSe and CdTe/CdSe QD-based QDSCs. (a) J–V, (b) IPCE, and (c) APCE curves.

photovoltaic parameters are collected in Table 1. It is noted that for the photovoltaic performance measurement at least three cells were constructed and evaluated in parallel, and both the average and recorded cell results are reported for the CdTe/CdSe-based cells in Table 1. Because CdTe QD proved to suffer from the problem of chemical stability and the photovoltaic performance of the corresponding cell device is quite poor,[12,45] CdTe QD-based cells were not selected for use as the reference.

Table 1. Photovoltaic Parameters for QDSCs Based on Different QD Sensitizers with Identical Particle Sizes

QDs	J_{sc} (mA cm^{-2})	V_{oc} (V)	FF (%)	PCE (%)
CdTe/CdSe[a]	19.59	0.606	0.569	6.76
CdTe/CdSe[b]	18.56	0.603	0.582	6.51
CdSe[b]	14.12	0.548	0.580	4.49

[a]Recorded efficiency device values. [b]Average values of the different devices.

The obtained PCE value (4.49%) for the reference CdSe QD-based cells is in the normal level compared to our recently published results.[12,14] In comparison, the FF values show no significant difference between the CdTe/CdSe- and CdSe-based cells; however, by taking into account the higher photocurrent of CdTe/CdSe and consequently the higher voltage drop at the series resistance, the core/shell QDs provide a better behavior from the point of view of the FF; the V_{oc} for the CdTe/CdSe cell (0.606 V) is slightly greater than those from CdSe (0.548 V), whereas the J_{sc} for the CdTe/CdSe cell (19.59 mA cm^{-2}) is significantly greater than that for CdSe (14.12 mA cm^{-2}). The higher J_{sc} value of the CdTe/CdSe cells in comparison with CdSe-based cells is mainly ascribed to the extension of the light-absorption range, as shown in the absorption spectra of Figure 2 and higher light-injection efficiency discussed below. The increased V_{oc} in the CdTe/CdSe cells can be ascribed to the higher J_{sc}. This feature follows from the standard diode eq 1

$$V_{oc} = \frac{k_B T}{q\beta}\left(\ln \frac{j_{sc}}{j_o} + 1\right) \quad (1)$$

where k_B is the Boltzmann constant, T is the temperature, q is the electron charge, β is a parameter related with the nonlinear recombination, and j_0 the diode dark current.[61] The higher j_{sc} value implies higher charge injection. If the recombination rate is the same in both cells (this point is clarified later by means of IS analysis), then larger j_{sc} values signify higher electron density at open circuit, which produces an increase in V_{oc}. The CdTe/CdSe-based cells exhibit the best performance, with J_{sc} = 19.59 mA cm^{-2}, V_{oc} = 0.606 V, FF = 0.569, and PCE = 6.76%. The obtained PCE of 6.76% is believed to be the best performance in the liquid-junction QDSCs so far. To compare this with other works in the literature, the record cell was also measured without a mask, obtaining J_{sc} = 22.01 mA cm^{-2}, V_{oc} = 0.613 V, FF = 0.564, and PCE = 7.61%. However, it is important to highlight that the measured data without applying a mask is not meaningful because the obtained J–V data are exaggerated and are not reproducible. Other efforts in solid-state heterojunction QDSCs based on Sb_2S_3, PbS, and $CH_3NH_3PbI_2$ have yielded PCE values in the range of 6–10%,[20,21,62,63] which also used different configurations in comparison with the sensitized solar cells. Our results reported here situate these state-of-the-art QDSCs in the same range as those produced by other technologies.

The photocurrent response to incident light was evaluated by IPCE. As shown in Figure 4b, the photocurrent response matches well the absorption profile, with photocurrent onsets at a wavelength of 700 nm for the CdSe and 930 nm for CdTe/CdSe-based solar cells, respectively. It is noted that the

dx.doi.org/10.1021/ja4079804 | J. Am. Chem. Soc. 2013, 135, 15913–15922

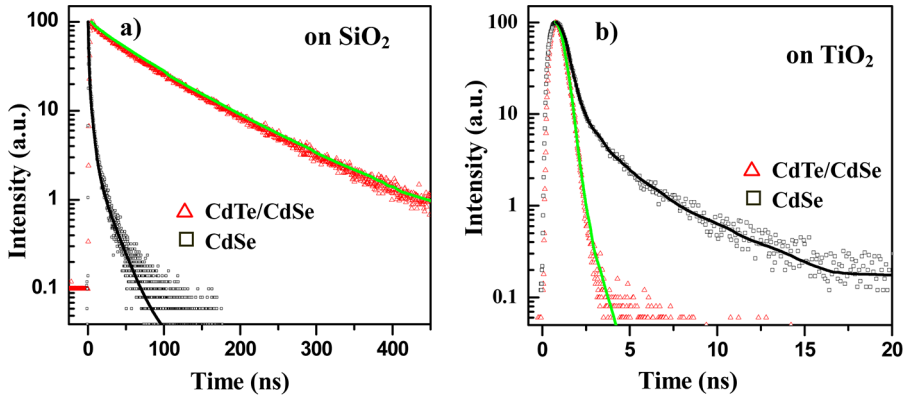

Figure 5. PL emission decay of CdTe/CdSe and reference CdSe QDs deposited on different substrates: (a) SiO_2 and (b) TiO_2 nanoparticulate films. The solid lines represent the kinetic fit using mono-, bi-, or triexponential decay analysis.

Table 2. Fit Parameters of PL Decay Curves of CdTe/CdSe and CdSe QDs Deposited on Different Substrates[a]

QDs	substrate	a_1	τ_1 (ns)	a_2	τ_2 (ns)	a_3	τ_3 (ns)	χ^2	$\langle\tau\rangle$ (ns)	k_{et} (10^9 s^{-1})
CdTe/CdSe	SiO_2	4515.00	73.26					0.997	73.26	1.91
	TiO_2	3434.9	0.52					0.978	0.52	
CdSe	SiO_2	81.64	0.78	24.73	4.07	3.22	18.80	1.16	7.11	0.52
	TiO_2	159.80	0.67	4.46	5.37			1.17	1.53	

[a]Determined using the fitting function $a_1 \exp(-t/\tau_1) + a_2 \exp(-t/\tau_2) + a_3 \exp(-t/\tau_3)$.

photoresponse range in the IPCE spectra is a little bit wider than the corresponding absorption range in the absorption spectra. This may be ascribed to the light-scattering effect by large-sized TiO_2 particles in the light-scattering layer for IPCE measurement.[12] IPCEs of ~80% in the range of 350−600 nm were observed for CdSe and CdTe/CdSe sensitizers, but a much broader response range (350−930 nm) was found for the CdTe/CdSe sensitizer in comparison with that for CdSe (350−650 nm). By integrating the product of the incident photon flux density and the cell's IPCE spectra, the calculated J_{sc} value for CdTe/CdSe- and CdSe-based solar cells are 18.42 and 13.69 mA cm^{-2}, respectively, which are close to the measured values shown in Table 1. Note that from 600 to 930 nm the IPCE for CdTe/CdSe is lower than 80%, the limit imposed by the reflection in the glass substrate. In this sense, there is room for further improvement of cell performance, at least from the point of view of the photocurrent.

We can see that the IPCE value for the CdSe-based cell in the short-wavelength range (400−600 nm) is a little higher than that of CdTe/CdSe. However, we cannot conclude that the electron collection and/or injection efficiency of CdSe is higher than that of CdTe/CdSe in this region because the IPCE value depends on a series of device parameters: IPCE = LHE × ϕ_{inj} × η_{cc}, where LHE is the light-harvesting efficiency, ϕ_{inj} is the electron-injection efficiency, and η_{cc} is the charge-collection efficiency. To examine more accurately the electron collection and/or injection efficiency for different sensitizers, the APCE (absorbed photon-to-electron conversion efficiency) was calculated according to the following equation: APCE(λ) = IPCE(λ)/[1 − $10^{-Abs(\lambda)}$], where Abs(λ) is the absorbance of photoanode at wavelength λ. The results are shown in Figure 4c.[64] This takes out the effect of the varying optical densities of the different electrodes. We can see that the APCE values corresponding to CdTe/CdSe-based cells are higher than that of CdSe-based cells in the range of 350−600 nm. This clearly demonstrates that the electron collection and/or injection efficiency of the CdTe/CdSe solar cells are higher than that of CdSe solar cells.

PL Emission Decay. It has been demonstrated that the excited-state features of QDs are dependent on the substrate to which they are attached.[65] When the highly luminescent CdTe/CdSe QDs are anchored onto TiO_2 mesoporous films, a significant quenching of the PL emission is observed (results not shown), thus confirming the excited-state interaction between the TiO_2 substrate and CdTe/CdSe particles. The quenching phenomenon demonstrates the deactivation of the excited QD via electron transfer to the TiO_2 substrate.[66] We further analyzed the excited CdTe/CdSe together with reference CdSe QDs deactivation by monitoring the PL decay (i.e., the exciton lifetimes). Transparent SiO_2 and TiO_2 oxide layers were prepared by screen printing corresponding colloidal pastes on FTO glass substrates followed by annealing at 500 °C. These obtained oxide films were then immersed in an MPA-capped QD aqueous dispersion to allow the self-assembly of QDs on the oxide substrates, as described for the preparation of sensitized TiO_2 film electrodes in the Experimental Section. This method allows for the direct bonding between the QDs and oxide substrate and also achieves monolayer coverage of QDs without aggregation.[66] Figure 5 shows the PL decay of CdTe/CdSe type-II core/shell QDs and reference CdSe QD deposition on an insular SiO_2 or TiO_2 film substrate, respectively. Mono-, bi-, or triexponential decay kinetics was found to be successful in fitting the lifetime traces, and the fit parameters are listed in Table 2. Average lifetimes of QD PL decay were calculated on the basis of these extracted values using eq 2

$$\langle\tau\rangle = \frac{\sum_n (a_n \tau_n^2)}{\sum_n (a_n \tau_n)} \quad (2)$$

where n corresponds to the nth component of a given multiexponential decay process.[67] It was found that when QDs were deposited on an insular SiO_2 substrate, the exciton

dx.doi.org/10.1021/ja4079804 | J. Am. Chem. Soc. 2013, 135, 15913−15922

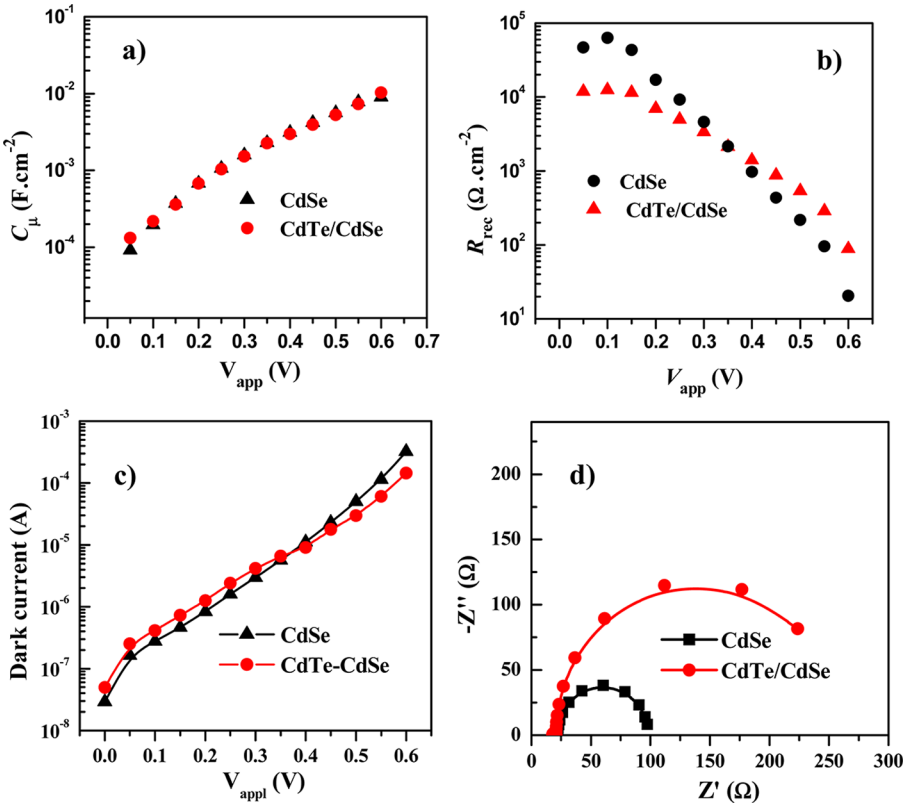

Figure 6. Impedance spectroscopy characterization of the CdTe/CdSe- and CdSe-based solar cells. (a) Chemical capacitance, C_μ, (b) recombination resistance, R_{rec}, and (c) dark currents as a function of applied voltage, V_{appl}. (d) Nyquist plots of the solar cells at −0.6 V forward bias.

lifetimes are quite longer (73.26 and 7.10 ns for the CdTe/CdSe and CdSe QDs, respectively) because the charge recombination dominates in this case. The longer exciton lifetime (73.26 ns) observed for CdTe/CdSe is due to the spatial separation of the charge carries (electron hole pair) in the type-II structure, and this long exciton lifetime gives a solid support for the assignment of a type-II structure to the obtained CdTe/CdSe QDs. Meanwhile, the monoexponential decay feature observed in CdTe/CdSe QDs reveals the high-quality optical properties as well as the decreased possibility of nonradiative recombination in the QDs. When QDs were deposited on the TiO_2 substrate, an additional deactivation route is created because electrons can easily inject into the TiO_2 substrate with a lower conduction band edge. Therefore, the corresponding exciton lifetimes decrease significantly to only 0.52 and 1.5 ns for CdTe/CdSe and CdSe QDs, respectively. Because the insular SiO_2 substrate does not accept electrons from the excited QDs, the shortening of the lifetime for QDs on TiO_2 is ascribed to electron injection to the TiO_2 substrate, the corresponding rate constant (k_{et}) of which can be obtained by eq 3

$$k_{et} = \frac{1}{\tau(\mathrm{QD/TiO_2})} - \frac{1}{\tau(\mathrm{OD/SiO_2})} \quad (3)$$

where $\tau_{(QD/TiO_2)}$ is the exciton lifetime of QDs on the TiO_2 substrate and $\tau_{(QD/SiO_2)}$ corresponds to the exciton lifetime of QDs on SiO_2. On the basis of the lifetimes listed in Table 2, the calculated electron-injection constants (k_{et}) are 1.91×10^9 and 0.52×10^9 s^{-1} for CdTe/CdSe and CdSe QDs assembled on TiO_2 substrates, respectively. It is noted that the observed k_{et} value for CdSe QDs in our case is in the same range as those observed previously.[43,46] The electron-injection constant of CdTe/CdSe QDs is significantly larger than that of CdSe QDs. This is due to the spatial separation of charge carriers (electron and hole, e−h pair) in the CdTe/CdSe type-II core/shell structure. This favors the electron injection into the substrate and minimizes the unwanted charge recombination. However, the localization of the hole inside the core region in a type-II structure does not favor the transfer of the hole and regeneration of neutral QDs from the oxidized form. Luckily, as described above, the thickness of the CdSe shell in our case is only 1.1 nm, which is thin enough for hole tunneling on the basis of a previous report.[59]

Impedance Spectroscopy (IS). To unveil the superior photovoltaic performance of the CdTe/CdSe-based solar cell in comparison with reference CdSe cells, we characterized the cell devices by IS and analyzed the data with the standard models for QDSCs.[17,23,36] IS measurements were carried out under dark conditions at a different forward bias ranging from 0 V to an applied voltage higher than V_{oc}, applying a 20 mV ac sinusoidal signal over the constant applied bias with the frequency ranging between 1 MHz and 0.1 Hz. It should be noted that $J-V$ curves (Figure S3) were performed both before and after IS measurements (a period of about 60 min) to verify the validity of the IS data obtained. The experimental results indicate that no significant variation in the photovoltaic parameters for both CdTe/CdSe- and CdSe-based QDSC was observed. This indicates that the stability of the CdTe/CdSe-based cell is comparable to that of the CdSe-based cell over this period of time. Nyquist curves for the CdTe/CdSe and CdSe QD-sensitized cells under different bias are given in Figure S4. The extracted values obtained for the chemical capacitance, C_μ, and recombination resistance, R_{rec}, are

dx.doi.org/10.1021/ja4079804 | J. Am. Chem. Soc. 2013, 135, 15913−15922

Table 3. Simulated Values of Resistance (R) and Capacitance (C) under the Forward Bias of −0.6 V for Cell Devices Based on CdTe/CdSe and CdSe QD Sensitizers

cells	R_s (Ω cm^2)	R_{CE} (Ω cm^2)	C_{CE} (μF cm^{-2})	R_{rec} (Ω cm^2)	C_μ (mF cm^{-2})	τ_n (ms)
CdSe	4.82	0.22	43.7	20.52	9.04	185.5
CdTe/CdSe	4.12	0.37	35.6	88.42	10.3	910.7

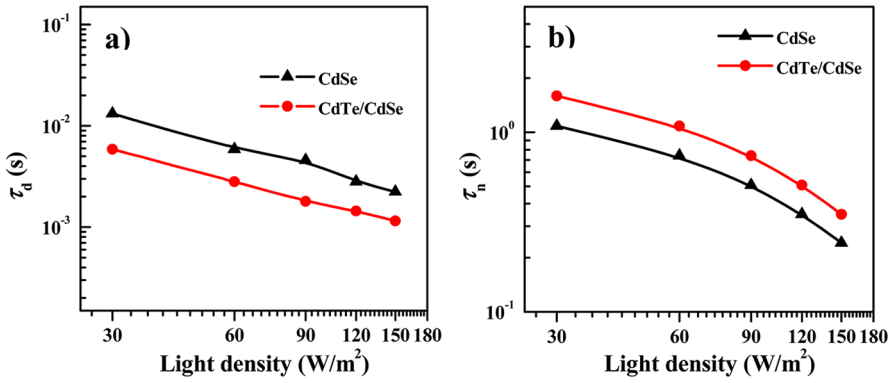

Figure 7. Dependenc of the electron transit time, τ_d (a), and electron lifetime, τ_n (b), of CdTe/CdSe- and CdSe-based solar cells on light densities in IMPS or IMVS measurement.

presented in Figure 6a,b. R_{rec} shunted with C_μ reflects the recombination resistance, related to the recombination of electrons at TiO_2 with acceptor species in the QDs and electrolyte.[17,23,36] The similar C_μ values obtained from both cells (Figure 6a) indicate that the nature of the different sensitizers (CdSe or CdTe/CdSe QDs) does not affect the level of the conduction band or the density of states of TiO_2.[23] However, there is an apparent difference in the R_{rec} values between the two cells. As shown in Figure 6b, when the forward bias is larger than 0.4 V at the region of maximum power provided by the cell, the R_{rec} values of the CdTe/CdSe cells are several times higher than those of the CdSe cells. For clarity, Figure 6d gives a direct comparison of the CdTe/CdSe and CdSe cells at a forward bias near the open-circuit voltage, 0.6 V, of the cells, and the extracted IS parameters are collected in Table 3. This comparison is correct because we have shown in Figure 6a that for the same applied bias the Fermi level is at the same position (same electron density for both cells). It was found that the R_{rec} value of the CdTe/CdSe solar cell (88.42 Ω cm^2) is more than 4 times higher than that of CdSe cells (20.52 Ω cm^2). The calculated electron lifetime ($\tau_n = R_{rec} \times C_\mu$) of the CdSe/CdS QDSC at this voltage is over 700 ms longer than that of the CdSe QDSC, supporting a lower recombination rate for the former, which is conducive to the increase of the η_{cc} and J_{sc} values in the CdTe/CdSe cell in comparison with the CdSe cell. Meanwhile, the dependence of the dark currents on the forward bias in the IS measurement are illustrated in Figure 6c. We found that the IS dark current−applied voltage curve of the CdSe cell is higher than that for the CdTe/CdSe solar cell at voltages higher than 0.4 V, as was observed for R_{rec}. This result points in the same direction as the impedance characterization, suggesting better blockage of charge recombination in the CdTe/CdSe cells.[15]

IMPS and IMVS have also been employed to estimate the electron transport and recombination dynamics in our constructed cell devices. In IMPS (or IMVS) measurements, the photocurrent and photovoltage response are used to evaluate electron transit time (τ_d) and electron lifetime (τ_n) in sensitized solar cells by the expression $\tau_d = (1/2)\pi f_{IMPS}$, and $\tau_n = (1/2)\pi f_{IMVS}$, where f_{IMPS} is the frequency of the minimum IMPS (IMVS) imaginary component.[68−70] As shown in Figure 7a,b, both τ_d and τ_n decrease with the increase in the light intensity. The IMPS results (Figure 7a) indicate clearly that the τ_d for the CdTe/CdSe cells (about 1.1−5.9 ms) is remarkably shorter than those for the reference CdSe solar cells (2.3−13.2 ms) at varied light intensities. This observation is related to the larger charge generation in the CdTe/CdSe cells, which brings forward an enhanced electron concentration in the TiO_2 substrate of the CdTe/CdSe cells compared to that of the CdSe cells.

The electron lifetime (τ_n) derived from the IMVS measurement (Figure 7b) reflects the recombination processes in the QDSCs. Direct measurements of the electron lifetime by IMVS are compared with the lifetime calculated from IS (Table 2). A good agreement between the lifetimes calculated by both techniques is obtained. The CdTe/CdSe QDSC shows a longer electron lifetime in comparison with CdSe. Similarly, the spatial separation of e−h pairs in the CdTe/CdSe type-II core/shell structure retards the charge-recombination rate and enhances the electron lifetime.

CONCLUSIONS

Highly efficient CdTe/CdSe QD-sensitized solar cells have been built by the direct covalent bonding of an MPA-capped QD sensitizer around TiO_2 mesoporous film electrodes. The type-II core/shell CdTe/CdSe QD extends its light-absorption range to the infrared because of the existence of an effective narrow band gap or an exciplex state formed between the valence band of CdTe and the conduction band of CdSe. The high surface coverage and uniform distribution of QD sensitizers throughout the film electrode thickness have been confirmed by EDX elemental mapping. An accelerated electron injection and a retarded charge recombination pathway in the built cell devices have been confirmed by APCE, IS, PL decay, IMPS, and IMVS characterizations. As a sensitizer in QDSCs, type-II CdTe/CdSe core/shell QDs are superior to plain CdSe QDs and possess the advantages of a broader light-harvesting range with an absorption onset extending to the infrared spectral window, an accelerated electron injection rate, and a retarded recombination rate because of the spatial separation of

dx.doi.org/10.1021/ja4079804 | J. Am. Chem. Soc. 2013, 135, 15913−15922

the electron−hole pair in the characteristic type-II structure. Therefore, constructing type-II core/shell-structured QDs is a promising way to develop panchromatic QD sensitizers for high-performance QDSCs. With the combination of the high-quality of the QD sensitizers and the effective deposition technique to ensure high surface coverage, a record PCE of 6.76% with a mask around the active film under illumination of full 1 sun was obtained, which is the highest reported value to date for a liquid-junction QDSC. This result situates the sensitized technology in the same range of efficiencies reported with other QD solar-cell configurations. Because of the low photovoltage resulting from the common polysulfide electrolyte used, the exploration of a suitable electrolyte to replace the polysulfide redox couple is one of the shortcuts to significantly enhance the PCE of QDSCs.

■ ASSOCIATED CONTENT

Supporting Information

UV−vis absorption and PL emission spectra of 4.9 nm sized CdSe and CdTe QDs, UV−vis absorption spectrum of CdTe/CdSe QDs before (oil-soluble) and after (water-soluble) phase transfer, *J*−*V* curves of CdTe/CdSe- and CdSe-based solar cells before and after IS measurements, and Nyquist plots of CdTe/CdSe- and CdSe-based solar cells. This material is available free of charge via the Internet at http://pubs.acs.org.

■ AUTHOR INFORMATION

Corresponding Author

zhongxh@ecust.edu.cn

Notes

The authors declare no competing financial interest.

■ ACKNOWLEDGMENTS

We acknowledge the National Natural Science Foundation of China (no. 21175043), the Science and Technology Commission of Shanghai Municipality (nos. 11JC1403100, 12NM0504101, and 12ZR1407700), and the Fundamental Research Funds for the Central Universities for financial support.

■ REFERENCES

(1) Barnham, K. W. J.; Mazzer, M.; Clive, B. *Nat. Mater.* **2006**, *5*, 161−164.
(2) Sambur, J. B.; Novet, T.; Parkinson, B. A. *Science* **2010**, *330*, 63−66.
(3) Semonin, O. E.; Luther, J. M.; Choi, S.; Chen, H.-Y.; Gao, J.; Nozik, A. J.; Beard, M. C. *Science* **2011**, *334*, 1530−1533.
(4) Pandey, A.; Guyot-Sionnest, P. *Science* **2008**, *322*, 929−932.
(5) Kamat, P. V. *J. Phys. Chem. C* **2008**, *112*, 18737−18753.
(6) Mora-Seró, I.; Bisquert, J. *J. Phys. Chem. Lett.* **2010**, *1*, 3046−3052.
(7) Ruhle, S.; Shalom, M.; Zaban, A. *ChemPhysChem* **2010**, *11*, 2290−2304.
(8) Kamat, P. V.; Tvrdy, K.; Baker, D. R.; Radich, J. G. *Chem. Rev.* **2010**, *110*, 6664−6688.
(9) Hetsch, F.; Xu, X.; Wang, H.; Kershaw, S. V.; Rogach, A. L. *J. Phys. Chem. Lett.* **2011**, *2*, 1879−1887.
(10) Kamat, P. V. *Acc. Chem. Res.* **2012**, *45*, 1906−1915.
(11) Kamat, P. V. *J. Phys. Chem. Lett.* **2013**, *4*, 908−918.
(12) Pan, Z.; Zhao, K.; Wang, J.; Zhang, H.; Feng, Y.; Zhong, X. *ACS Nano* **2013**, *7*, 5215−5222.
(13) Pan, Z.; Zhang, H.; Cheng, K.; Hou, Y.; Hua, J.; Zhong, X. *ACS Nano* **2012**, *6*, 3982−3991.
(14) Zhang, H.; Cheng, K.; Hou, Y.; Fang, Z.; Pan, Z.; Wu, W.; Hua, J.; Zhong, X. *Chem. Commun.* **2012**, *48*, 11235−11237.
(15) Yan, K.; Zhang, L.; Qiu, J.; Qiu, Y.; Zhu, Z.; Wang, J.; Yang, S. *J. Am. Chem. Soc.* **2013**, *135*, 9531−9539.
(16) Santra, P. K.; Kamat, P. V. *J. Am. Chem. Soc.* **2012**, *134*, 2508−2511.
(17) Hossain, Md. A.; Jennings, J. R.; Shen, C.; Pan, J. H.; Koh, Z. Y.; Mathews, N.; Wang, Q. *J. Mater. Chem.* **2012**, *22*, 16235−16242.
(18) Sung, S. D.; Lim, I.; Kang, P.; Lee, C.; Lee, W. I. *Chem. Commun.* **2013**, *49*, 6054−6056.
(19) Luo, J.; Wei, H.; Huang, Q.; Hu, X.; Zhao, H.; Yu, R.; Li, D.; Luo, Y.; Meng, Q. *Chem. Commun.* **2013**, *49*, 3881−3883.
(20) Im, S. H.; Lim, C.-S.; Chang, J. A.; Lee, Y. H.; Maiti, N.; Kim, H.-J.; Nazeeruddin, Md. K.; Gratzel, M.; Seok, S. I. *Nano Lett.* **2011**, *11*, 4789−4793.
(21) Ip, A. H.; Thon, S. M.; Hoogland, S.; Voznyy, O.; Zhitomirsky, D.; Debnath, R.; Levina, L.; Rollny, L. R.; Carey, G. H.; Fischer, A.; Kemp, K. W.; Kramer, I. J.; Ning, Z.; Labelle, A. J.; Chou, K. W.; Amassian, A.; Sargent, E. H. *Nat. Nanotechnol.* **2012**, *7*, 577−582.
(22) Hodes, G. *J. Phys. Chem. C* **2008**, *112*, 17778−17787.
(23) Mora-Seró, I.; Gimenez, S.; Fabregat-Santiago, F.; Gomez, R.; Shen, Q.; Toyoda, T.; Bisquert, J. *Acc. Chem. Res.* **2009**, *42*, 1848−1857.
(24) Robel, I.; Subramanian, V.; Kuno, M.; Kamat, P. V. *J. Am. Chem. Soc.* **2006**, *128*, 2385−2393.
(25) Robel, I.; Kuno, M.; Kamat, P. V. *J. Am. Chem. Soc.* **2007**, *129*, 4136−4137.
(26) Kim, S.; Fisher, B.; Eisler, H. J.; Bawendi, M. *J. Am. Chem. Soc.* **2003**, *125*, 11466−11467.
(27) Zhu, H.; Song, N.; Lian, T. *J. Am. Chem. Soc.* **2011**, *133*, 8762−8771.
(28) Lo, S. S.; Mirkovic, T.; Chuang, C. H.; Burda, C.; Scholes, G. D. *Adv. Mater.* **2011**, *23*, 180−197.
(29) Scholes, G. D.; Jones, M.; Kumar, S. *J. Phys. Chem. C* **2007**, *111*, 13777−13785.
(30) Itzhakov, S.; Shen, H.; Buhbut, S.; Lin, H.; Oron, D. *J. Phys. Chem. C* [Online early access]. DOI: 10.1021/jp312190x. Published Online: Dec 20, **2012**.
(31) Zhong, H.; Zhou, Y.; Yang, Y.; Yang, C.; Li, Y. *J. Phys. Chem. C* **2007**, *111*, 6538−6543.
(32) Ning, Z.; Tian, H.; Yuan, C.; Fu, Y.; Qin, H.; Sun, L.; Agren, H. *Chem. Commun.* **2011**, *47*, 1536−1538.
(33) Bang, J.; Park, J.; Lee, J. H.; Won, N.; Nam, J.; Lim, J.; Chang, B. Y.; Lee, H. J.; Chon, B.; Shin, J.; Park, J. B.; Choi, J. H.; Cho, K.; Park, S. M.; Joo, T.; Kim, S. *Chem. Mater.* **2010**, *22*, 233−240.
(34) Tang, J.; Sargent, E. H. *Adv. Mater.* **2011**, *23*, 12−29.
(35) Lai, C.-H.; Chou, P.-T. *Chem. Commun.* **2011**, *47*, 3448−3450.
(36) González-Pedro, V.; Xu, X.; Mora-Seró, I.; Bisquert, J. *ACS Nano* **2010**, *4*, 5783−5790.
(37) Li, L.; Yang, X.; Gao, J.; Tian, H.; Zhao, J.; Hagfeldt, A.; Sun, L. *J. Am. Chem. Soc.* **2011**, *133*, 8458−8460.
(38) Wang, H.; Luan, C.; Xu, X.; Kershaw, S. V.; Rogach, A. L. *J. Phys. Chem. C* **2012**, *116*, 484−489.
(39) Yu, X.; Lei, B.; Kuang, D.; Su, C. *J. Mater. Chem.* **2012**, *22*, 12058−12063.
(40) Zhang, Q.; Guo, X.; Huang, X.; Huang, S.; Li, D.; Luo, Y.; Shen, Q.; Toyoda, T.; Meng, Q. *Phys. Chem. Chem. Phys.* **2011**, *13*, 4659−4667.
(41) Tian, J.; Gao, R.; Zhang, Q.; Zhang, S.; Li, Y.; Lan, J.; Qu, X.; Cao, G. *J. Phys. Chem. C* **2012**, *116*, 18655−18662.
(42) Giménez, S.; Mora-Seró, I.; Macor, L.; Guijarro, N.; Lana-Villarreal, T.; Goméz, R.; Diguna, L. J.; Shen, Q.; Toyoda, T.; Bisquert, J. *Nanotechnology* **2009**, *20*, 295204.
(43) Kongkanand, A.; Tvrdy, K.; Takechi, K.; Kuno, M.; Kamat, P. V. *J. Am. Chem. Soc.* **2008**, *130*, 4007−4015.
(44) Mora-Seró, I.; Giménez, S.; Moehl, T.; Fabregat-Santiago, F.; Lana-Villareal, T.; Gómez, R.; Bisquert, J. *Nanotechnology* **2008**, *19*, 424007.
(45) Bang, J. H.; Kamat, P. V. *ACS Nano* **2009**, *3*, 1467−1476.

(46) Ning, Z.; Tian, H.; Qin, H.; Zhang, Q.; Ågren, H.; Sun, L.; Fu, Y. *J. Phys. Chem. C* **2010**, *114*, 15184−15189.
(47) Chen, J.; Zhao, D. W.; Song, J. L.; Sun, X. W.; Deng, W. Q.; Liu, X. W.; Lei, W. *Electrochem. Commun.* **2009**, *11*, 2265−2267.
(48) Salant, A.; Shalom, M.; Hod, I.; Faust, A.; Zeban, A.; Banin, U. *ACS Nano* **2010**, *4*, 5962−5968.
(49) Salant, A.; Shalom, M.; Tachan, Z.; Buhbut, S.; Zaban, A.; Banin, U. *Nano Lett.* **2012**, *12*, 2095−2100.
(50) Santra, P. K.; Kamat, P. V. *J. Am. Chem. Soc.* **2013**, *135*, 877−885.
(51) Watson, D. F. *J. Phys. Chem. Lett.* **2010**, *1*, 2299−2309.
(52) Zhang, W.; Chen, G.; Wang, J.; Ye, B.-C.; Zhong, X. *Inorg. Chem.* **2009**, *48*, 9723−9731.
(53) Yu, W. W.; Wang, A.; Peng, X. G. *Chem. Mater.* **2003**, *15*, 4300−4308.
(54) Zhong, X.; Feng, Y.; Zhang, Y. *J. Phys. Chem. C* **2007**, *111*, 526−531.
(55) Liu, L.; Zhong, X. *Chem. Commun.* **2012**, *48*, 5718−5720.
(56) Lee, H. J.; Bang, J.; Park, J.; Kim, S.; Park, S.-M. *Chem. Mater.* **2010**, *22*, 5636−5643.
(57) Smith, A. M.; Mohs, A. M.; Nie, S. *Nat. Nanotechnol.* **2009**, *4*, 56−63.
(58) King, L. A.; Riley, D. J. *J. Phys. Chem. C* **2012**, *116*, 3349−3355.
(59) Shen, Q.; Kobayashi, J.; Diguna, L. J.; Toyoda, T. *J. Appl. Phys.* **2008**, *103*, 084304-1−084304-5.
(60) Guijarro, N.; Campina, J. M.; Shen, Q.; Toyoda, T.; Lana-Villarreala, T.; Gomez, R. *Phys. Chem. Chem. Phys.* **2011**, *13*, 12024−12032.
(61) Fabregat-Santiago, F.; Garcia-Belmonte, G.; Mora-Seró, I.; Bisquert, J. *Phys. Chem. Chem. Phys.* **2011**, *13*, 9083−9118.
(62) Lee, M. M.; Teuscher, J.; Miyasaka, T.; Murakami, T. N.; Snaith, H. J. *Science* **2012**, *338*, 643−647.
(63) Kim, H.-S.; Lee, C.-R.; Im, J.-H.; Lee, K.-B.; Moehl, T.; Marchioro, A.; Moon, S.-J.; Humphry-Baker, R.; Yum, J.-H.; Moser, J. E.; Gratzel, M.; Park, N.-G. *Sci. Rep.* **2012**, *2*, 591.
(64) Fillinger, A.; Parkinson, B. A. *J. Electrochem. Soc.* **1999**, *146*, 4559−4564.
(65) Tvrdy, K.; Frantszov, P.; Kamat, P. V. *Proc. Natl. Acad. Sci. U.S.A.* **2011**, *108*, 29−34.
(66) Pernik, D.; Tvrdy, K.; Radich, J. G.; Kamat, P. V. *J. Phys. Chem. C* **2011**, *115*, 13511−13519.
(67) James, D. R.; Liu, Y.-S.; De Mayo, P.; Ware, W. R. *Chem. Phys. Lett.* **1985**, *120*, 460−465.
(68) Yu, X.-Y.; Liao, J.-Y.; Qiu, K.-Q.; Kuang, D.-B.; Su, C.-Y. *ACS Nano* **2011**, *12*, 9494−9500.
(69) Hsiao, P. T.; Tung, Y. L.; Teng, H. S. *J. Phys. Chem. C* **2010**, *114*, 6762−6769.
(70) Kruger, J.; Plass, R.; Gratzel, M.; Cameron, P. J.; Peter, L. M. *J. Phys. Chem. B* **2003**, *107*, 7536−7539.